High-temperature strength of directionally reinforced LaB$_6$–TiB$_2$ composite

I. Bogomol [a,b,*], T. Nishimura [b], O. Vasylkiv [b], Y. Sakka [b], P. Loboda [a]

[a] *National Technical University of Ukraine "KPI", Peremogy av. 37, Kyiv 03056, Ukraine*
[b] *Nano Ceramics Center, National Institute for Materials Science, 1-2-1, Sengen, Tsukuba, Ibaraki 305-0047, Japan*

ARTICLE INFO

ABSTRACT

A directionally solidified eutectic LaB$_6$–TiB$_2$ composite was prepared by the floating zone method based on the crucible-free zone melting of compacted powders. TiB$_2$ and LaB$_6$ powders were used as the initial materials. The bending strength of the melted eutectic LaB$_6$–TiB$_2$ composite was evaluated in the temperature range of 1000–1600 °C and reached 470 MPa at 1400 °C. We speculate that the bending strength of the directionally reinforced LaB$_6$–TiB$_2$ composite at high temperatures mainly depends on the plasticity of the TiB$_2$ fibers and LaB$_6$ matrix. By analyzing the dislocation structure of the fibers, the occurrence of strain hardening in monocrystalline titanium diboride during high-temperature deformation was revealed.

© 2010 Elsevier B.V. All rights reserved.

1. Introduction

It is well known that boride ceramics have a high melting point, hardness, creep resistance and sufficient chemical stability at elevated temperatures. These ceramics are used in functional and structural components in electronics operating at fast heating-cooling cycles and thermal tensions at temperatures up to 2000 °C.

Hot pressing is used for obtainment of such materials but this method is inadequate for achieving of high purity and structure perfection which are crucially important for functional materials [1–5]. Employing directional crystallization of the boride systems enable one to fabricate high purity self-reinforced composites which consist of ceramic matrix reinforced by ceramic inclusions with advanced mechanical properties when compared to monolithic borides [6–14].

The directionally crystallized eutectic alloys of LaB$_6$–Me^{IV}B$_2$ (Me^{IV}–Ti, Zr, Hf) are the most investigated ceramic materials in this field [6,10,12,15]. Electron diffraction studies [6–9] of the structure of the LaB$_6$–ZrB$_2$ alloy have shown that the reinforcing zirconium diboride fibers are monocrystalline and grow mainly in the $\langle 0\,0\,0\,1 \rangle$ direction. The ZrB$_2$ fiber with diameter of 0.2–0.8 μm and length of 500 μm has almost perfect hexagonal cross section.

Bending strength, in particular the high-temperature bending strength, is one of the main parameters which evaluate mechanical properties of these materials. In most previous studies of LaB$_6$-based ceramics, it was investigated only at room temperature [6,8,16], and the mechanical properties of fiber-reinforced zone-melted lanthanum hexaboride have not been evaluated at high temperatures, to the best of our knowledge.

In this paper, we produced, by a proprietary floating zone method, pure, directionally crystallized lanthanum hexaboride ceramics reinforced by TiB$_2$ fibers, and characterized the bending strength of this material in the temperature range 1000–1600 °C.

2. Experimental details

Directionally reinforced LaB$_6$–TiB$_2$ composites were obtained by the original floating zone method, developed at the National Technical University of Ukraine (NTUU "KPI") [12,13]. It is based on crucible-free zone melting of compacted powders. The powder mixture is pressed at room temperature into a pellet. This process is much easier and faster than the traditional high-pressure high-temperature (HPHT) sintering, but it produces relatively porous pellets. An "impurity solvent" is added to the initial powder mixture; its melting temperature is lower than the melting temperature of the main component. During the zone melting, the impurity solvent moves along the temperature gradient through the pores in the compacted powder [17]. This diffusion allows to achieve, in one step, both densification of the pellet and its refinement by the zone melting [12,17].

Commercial LaB$_6$ and TiB$_2$ powders (purity 98 wt%, average grain size 1 μm, Reaktiv Co Donetsk, Ukraine) were mixed according to ratios: 85 wt% LaB$_6$–15 wt% TiB$_2$, in accordance with phase diagrams [16]. One volume percent of boron powder (purity 99.8 wt%, particle size 0.5 μm) was added as the impurity solvent. The powders were mixed by sifting them 7 times through a 50 μm mesh. Polyvinyl alcohol was added as a plasticizer. Green rods with a diameter of 10 mm and length of 145 mm were obtained by compressing the mixture in a hydraulic press at 50 MPa. They were dried in a vacuum oven for 12 h at 100 °C and then, placed in the crystal-growth setup "Crystal 206" (Russia), equipped with an induction-type heater. An appropriate LaB$_6$ monocrystalline seeds with crystallographic orientations $\langle 1\,0\,0 \rangle$, $\langle 1\,1\,0 \rangle$ and $\langle 1\,1\,1 \rangle$ were added to obtain monocrystalline samples. Zone melting was

carried out in helium atmosphere at excess pressure of 1 atm. The growth rate was fixed at 5 mm/min.

For analysis, the composite samples were cut into rectangular 2.5 mm × 3 mm × 20 mm blocks by a spark-erosive cutter. Their lateral surfaces were ground and polished using diamond pastes. The microstructure and fracture surface of the directionally reinforced LaB_6–TiB_2 composites was studied using a scanning electron microscope (SEM) "Hitachi S4800" (Japan), equipped with an energy-dispersive X-ray spectrometer (EDS). The latter allows mapping the elemental composition inside SEM. Characterization of the strained and strain-free TiB_2 fibers was done by transmission electron microscopy (TEM) "Selmi ПЭМ 125К" (Ukraine).

The three-point bending strength tests were conducted at temperatures of 1000, 1200, 1400 and 1600 °C, in vacuum 1.3×10^{-3} Pa, using an "Instron 4505" setup (USA). The specimens of 3 mm × 2.5 mm × 20 mm were placed into graphite containers on the SiC supports spaced by 16 mm span. The graphite containers were chambered on the turn table of the testing machine. After evacuation, specimens were fed, by turn, into heating area for bending strength test operation. The loading speed was 0.5 mm/min. Four to six samples with ⟨1 0 0⟩, ⟨1 1 0⟩ and ⟨1 1 1⟩ crystallographic orientations of the LaB_6 matrix were tested at each temperature and the measurement accuracy was taken as the standard deviation.

3. Results and discussion

3.1. Elemental analysis

SEM-EDS analysis of a polished surface of the directionally crystallized eutectic LaB_6–TiB_2 composite reveals that it consists of a LaB_6 matrix reinforced with TiB_2 fibers (Fig. 1); the presence of Ti in the fibers is displayed in yellow in the map in Fig. 1(b). A representative EDS spectrum (Fig. 1(a)) shows Ti peaks at high energies and a strong signal originating from B and La.

3.2. Temperature dependence of bending strength

Fig. 2 shows the bending strength of the directionally reinforced LaB_6–TiB_2 composite as a function of temperature. In the temperature range of 1000–1600 °C the highest strength (470 MPa) is observed for the composite grown with the ⟨1 0 0⟩ orientation of the LaB_6 matrix phase and the lowest strength (350 MPa) is observed for the composite grown with the ⟨1 1 0⟩ orientation. Also bending strength decreases above the maximum temperature (1400 °C) for the composite grown with the ⟨1 0 0⟩ orientation and above the minimum temperature (1200 °C) for the composite grown with the ⟨1 1 0⟩ orientation.

3.3. Fracture analysis and relationship with dislocation gliding

Fig. 3(a) and (b) shows the LaB_6–TiB_2 samples grown in the ⟨1 0 0⟩ crystallographic orientation after fracturing at 1000 and 1600 °C, respectively demonstrating that the roughness of the fractured surface decreases with increasing testing temperature. At temperatures of 1200 °C and above the fracture occurs almost perpendicular to the long axis of the sample, correlated with the (1 0 0) plane of the LaB_6 matrix. Thus, we should suppose that at elevated temperatures the crack propagates along the planes of dislocation gliding in the matrix and the fibers are pulled out or broken.

The mechanism by which fibers are pulled out from the matrix greatly depends on the matrix–fiber interface strength and perfection. Therefore estimation of the mode of deformation of each phase during testing is very important. The thermal expansion coefficient is smaller for LaB_6 (6.4×10^{-6} K^{-1}) than for TiB_2 (7.6–8.6×10^{-6} K^{-1}) at all temperatures [18,19]. Therefore, after high-temperature zone melting and cooling to room temperature, compressive and tensile stresses should appear in the LaB_6 matrix and TiB_2 fibers, respectively. At room temperature the internal stresses characterize the composite strength. At elevated temperatures these stresses are decreased, and the fibers are more often pulled out from the fracture surface (Fig. 4). Thus, the composite strength should decrease. However, the experimental data indicates increasing bending strength with temperature (Fig. 2).
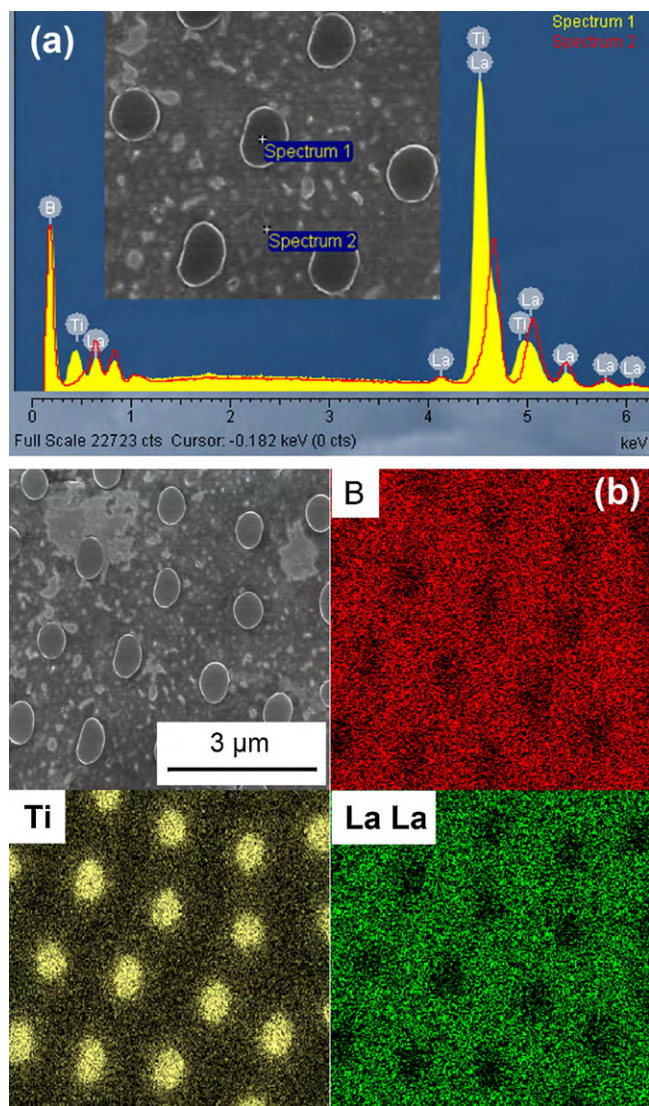
Fig. 1. EDS spectra (Spectrum 1: TiB_2, Spectrum 2: LaB_6) and mapping of the LaB_6–TiB_2 composite.
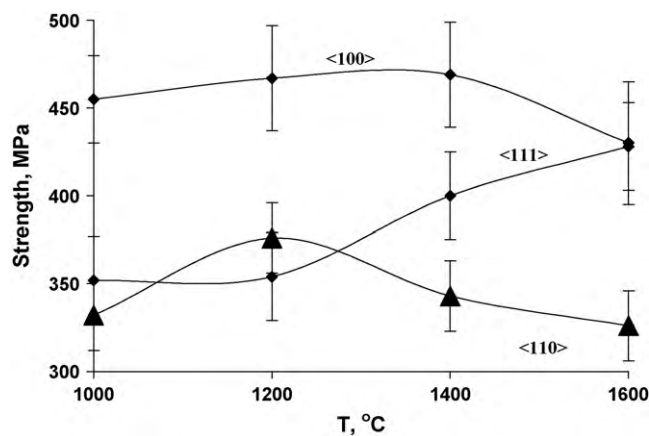
Fig. 2. Temperature dependence of bending strength of the directionally crystallized LaB_6–TiB_2 composite grown with different crystallographic directions of the matrix phase.
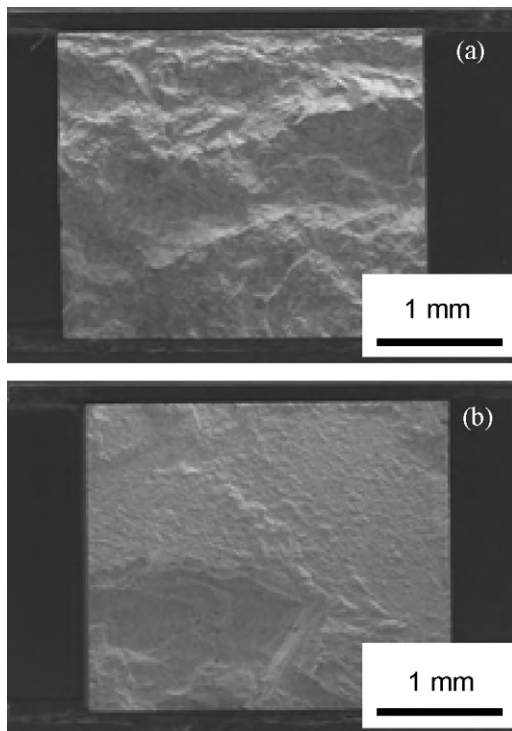
Fig. 3. Macrographs of fractures of the directionally reinforced LaB_6–TiB_2 composite grown in $\langle 1\,0\,0 \rangle$ crystallographic orientation at testing temperatures of (a) 1000 °C and (b) 1600 °C.

The high-temperature strength of composites also depends on the plasticity of the matrix and inclusions. The neck formation and holes in the LaB_6 matrix shown in the SEM micrograph of the LaB_6–TiB_2 surface fractured at 1000 °C (Fig. 4(a)) indicate that the plastic deformation of TiB_2 fibers occur before the fracture. At a testing temperature of 1200 °C (Fig. 4(b)) the slip lines are also observed in the LaB_6 matrix phase. Subsequent increases in the testing temperature to 1400–1600 °C (Fig. 4(c) and (d)) leads to an increase in dislocation line density in the matrix and increasing plasticity of the fibers.

The lanthanum hexaboride matrix has a cubic ($Pm3m$) crystallographic structure, whereas titanium diboride is hexagonal ($P6/mmm$) [18,19]. Therefore dislocations most easily glide in the $(0\,0\,0\,1)$ plane and the $\langle 1\,1\,2\,0 \rangle$ direction of TiB_2, i.e., normal to the sample axis; however, different slip systems $((1\,0\,1\,0)\,\langle 1\,1\,2\,0 \rangle$; $(1\,1\,0\,0)\,\langle 0\,0\,0\,1 \rangle$; $(1\,0\,1\,0)\,\langle 1\,1\,2\,1 \rangle)$ are also possible [20,21]. For LaB_6, dislocations most easily glide in the $(1\,1\,0)$ plane and the $\langle 1\,1\,1 \rangle$ crystallographic direction [21], which are tilted relative to the sample axis depending on the growth direction.

Because distinct equilibrium phase boundaries (the eutectic composite is solidified under near-equilibrium conditions) are observed for directionally solidified eutectic composites [22–24], we should say about similar grain-boundary strengthening [23,25,26]. Thus, the following two effects occurred at elevated temperatures:

(1) The effect of deformation resistance, explained by the difference in the slip systems of the lanthanum hexaboride matrix and titanium diboride fibers.
(2) The barrier effect, explained by barrier role of the boundary at dislocations gliding.

The second effect always occurs with plastic deformation. The first effect strongly depends on the coincidence of slip planes in the matrix and fiber phases. In our case, the resistance to defor-
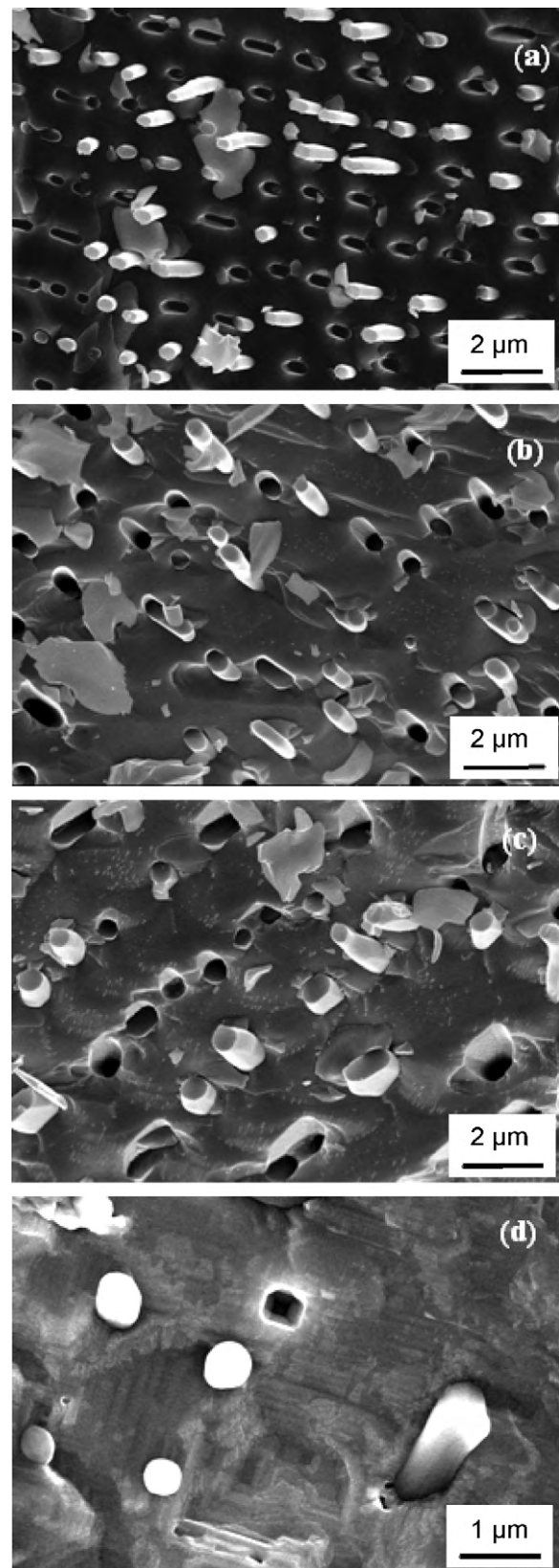
Fig. 4. Micrographs of fractures of the directionally reinforced LaB_6–TiB_2 composite grown in $\langle 1\,0\,0 \rangle$ crystallographic orientation at testing temperatures of (a) 1000 °C, (b) 1200 °C, (c) 1400 °C and (d) 1600 °C.

mation depends on the crystallographic orientation of the LaB_6 matrix phase because TiB_2 fibers grow mainly along the $\langle 0\,0\,0\,1 \rangle$ crystalline direction [6–9]. Thus, plastic deformation may occur in three different ways:

1. For the directionally reinforced LaB_6–TiB_2 composite grown in the $\langle 1\,1\,0 \rangle$ direction the coincidence of the slip planes in the matrix $(1\,1\,0)$ and fiber $(0\,0\,0\,1)$ phases is maximum [20,21]. Therefore, the mutual plastic deformation occurs most easily and fracture resistance is minimal especially at temperature higher $1200\,^\circ$C. As a result, the high-temperature bending strength of such alloy decreases in the temperature range of 1400–$1600\,^\circ$C (Fig. 2).
2. In the case of LaB_6–TiB_2 composite grown in the $\langle 1\,1\,1 \rangle$ direction, the $(0\,0\,0\,1)$ plane in the TiB_2 fiber is tilted at an angle to the $(1\,1\,0)$ plane in the LaB_6 matrix. Therefore, the mutual plastic deformation is complicated and the bending strength is increased (Fig. 2).
3. For the LaB_6–TiB_2 composite grown in the $\langle 1\,0\,0 \rangle$ direction, the $(0\,0\,0\,1)$ plane in the TiB_2 fiber is tilted at 45° (the maximum angle) to the $(1\,1\,0)$ plane in the LaB_6 matrix and the mutual plastic deformation has maximum complexity. As a result, the high-temperature bending strength of the directionally reinforced LaB_6–TiB_2 composite grown in the $\langle 1\,0\,0 \rangle$ direction is greater than that of composites grown in the $\langle 1\,1\,0 \rangle$ and $\langle 1\,1\,1 \rangle$ directions (Fig. 2). The decreasing strength of composite grown in the $\langle 1\,0\,0 \rangle$ direction at $1600\,^\circ$C (Fig. 2) is associated with decreasing plastic deformation resistance of the LaB_6 matrix phase and beginning of intensive plastic deformation in composite (Fig. 4(d)).

Thus, this observation reveals the importance of the relative inclination of planes along which dislocation gliding occurs most easily in explaining the high-temperature mechanical properties of fiber-reinforced ceramics [13,25]. At the same time, because of the high purity of the directionally crystallized composites, the plastic deformation of titanium diboride fibers can reach 60% (Figs. Fig. 4 and 5(a)), depending on the growth direction and testing temperature. Fig. 5(b) shows the relative reduction of area of TiB_2 fibers at high temperatures. The data is obtained by calculating the ratio of the neck and original fiber areas on the fracture surfaces of the composite grown with different crystallographic directions of the matrix phase.

3.4. High-temperature plasticity of the titanium diboride fibers

The investigation of the fracture surface by TEM shows that the dislocation arrangement appears in strained monocrystalline TiB_2 fibers (Fig. 6(a)) in contrast to in strain-free fibers (Fig. 6(b)). The strained fibers are being divided into regions with different directions of dislocation lines (Fig. 6(a)). Thus, the evolution of the dislocation arrangement of monocrystalline titanium diboride during high-temperature deformation was observed. This finding indicates that fiber plasticity is due to the gliding of dislocations, and accordingly, the mutual displacement or rotation of some regions (Figs. 6 and 7).

In region I in Fig. 6(a) near the matrix phase, dislocation lines oriented normal to the fiber axis are observed, which correspond to the $(0\,0\,0\,1)$ slip plane of the hexagonal ($P6/mmm$) crystallographic structure of titanium diboride (Fig. 7(a) and (b)) [20,21]. In this region, fibers are under shear stress parallel to the load direction. In region II in Fig. 6(a) the rate of deformation is higher and the strain is less homogeneous. The fibers are subjected to stretching strain and the $(1\,0\,\bar{1}\,0)$ planes parallel to the fiber axis undergo slippage. In this region the oriented cellular substructure typical of a multiple slip (twinning) is formed (Fig. 7(c) and (d)). Finally, in region III in
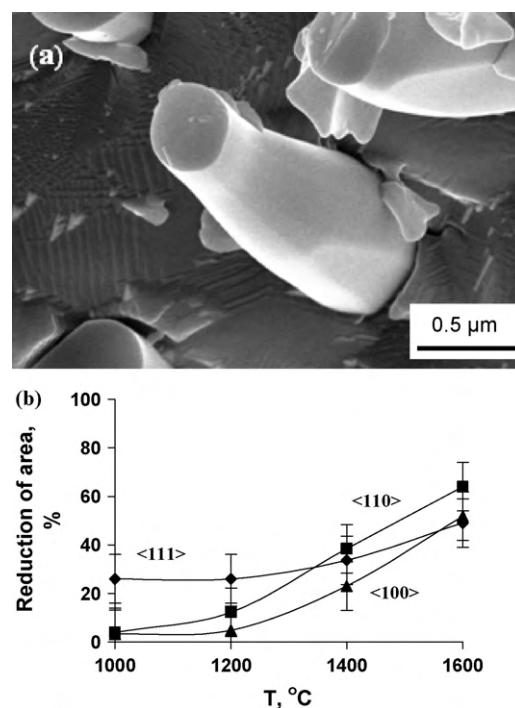
Fig. 5. Micrograph of strained TiB_2 fiber (a) and temperature dependence of the relative reduction of area of titanium diboride fibers in high-temperature bending strength test of the directionally crystallized LaB_6–TiB_2 composite grown with different crystallographic directions of the matrix phase (b).
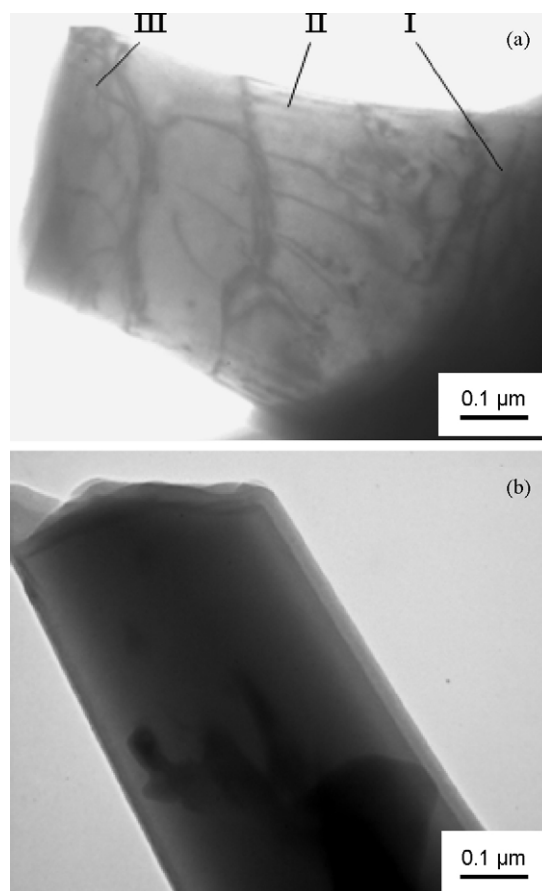
Fig. 6. TEM images of microstructure of (a) strained TiB_2 fibers at $1400\,^\circ$C and (b) strain-free TiB_2 fibers in the directly reinforced LaB_6–TiB_2 composite.
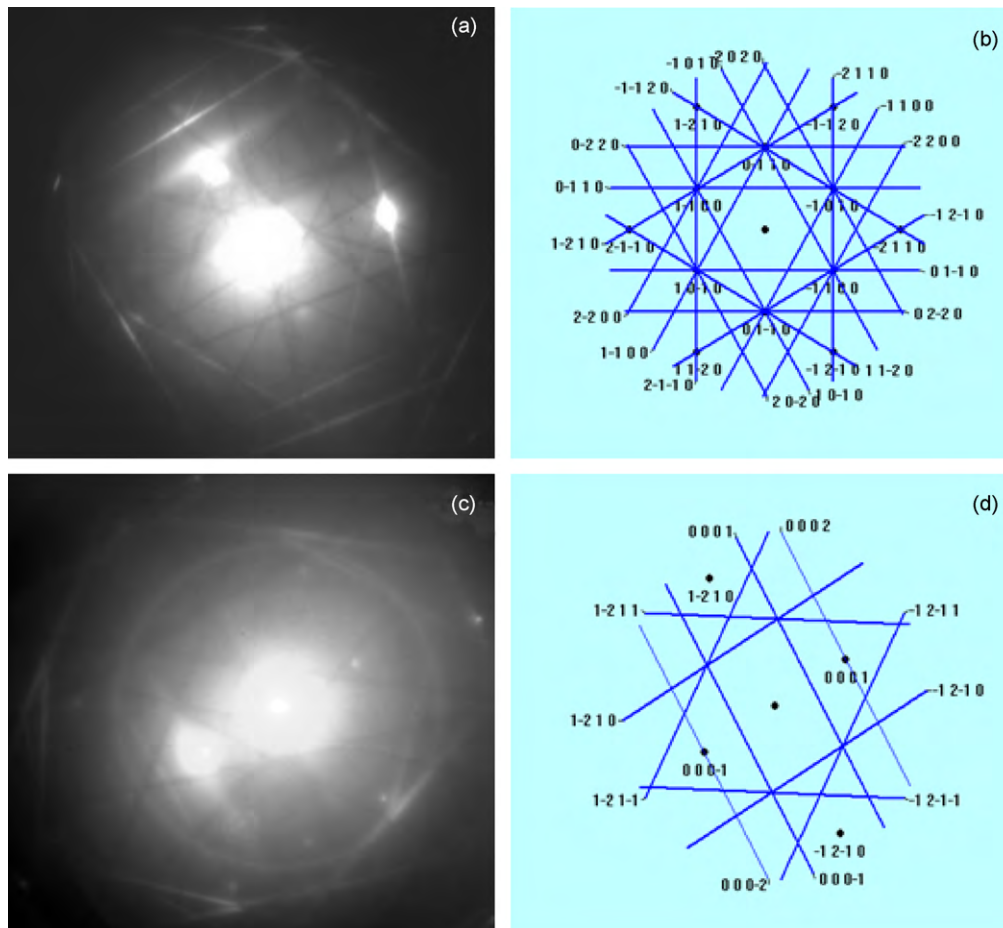
Fig. 7. Electron diffraction patterns (a and c) and interpretation (b and d) of region I (a and b) and region II (c and d) of strained TiB$_2$ fiber.

Fig. 6(a) near the fiber fracture, the dislocation density increases to 10^9 cm^{-2} and the disoriented cellular substructure is observed.

The structure nonuniformity of strained TiB$_2$ fibers (Fig. 6(a)) in contrast to strain-free fibers (Fig. 6(b)) demonstrates two facts:

(1) The monocrystalline titanium diboride fibers in the directly reinforced LaB$_6$–TiB$_2$ composite undergo plastic fracture at high temperatures (1000–1600 °C).
(2) During high-temperature deformation, the strain hardening of TiB$_2$ fibers is observed [25].

4. Conclusions

Directionally crystallized eutectic LaB$_6$–TiB$_2$ composites were obtained by the floating zone method, based on the crucible-free zone melting of compacted powders. The bending strength of the composite changed with increasing temperature in the range of 1000–1600 °C and reached 470 MPa at 1400 °C for the alloy grown in the ⟨1 0 0⟩ direction. The increasing composite strength at elevated temperatures is associated with increasing plasticity of the LaB$_6$ matrix and TiB$_2$ fibers.

References

[1] S.-Q. Zheng, H.-S. Yu, C.-T. Du, G.-H. Min, Z.-D. Zou, J. Mater. Sci. Lett. 21 (2002) 1829–1831.
[2] R. Gao, G. Min, H. Yu, S. Zheng, Q. Lu, J. Han, W. Wang, Ceram. Int. 31 (2005) 15–19.
[3] Yu.G. Tkachenko, D.Z. Yurchenko, V.K. Sul'zhenko, G.S. Oleinik, V.M. Vereshchaka, Powder Metall. Met. Ceram. 46 (5–6) (2007) 254–260.
[4] A.A. Shul'zhenko, D.A. Stratiichuk, G.S. Oleinik, N.N. Belyavina, V.Ya. Markiv, Powder Metall. Met. Ceram. 44 (1–2) (2005) 75–83.
[5] G. Min, R. Gao, H. Yu, J. Han, Key Eng. Mater. 297–300 (2005) 1630–1638.
[6] Yu. Paderno, V. Paderno, V. Filippov, J. Solid State Chem. 154 (1) (2000) 165–167.
[7] Yu. Paderno, V. Paderno, N. Shitsevalova, V. Filippov, J. Alloys Compd. 317–318 (2001) 367–371.
[8] H. Deng, E.C. Dickey, Y. Paderno, V. Paderno, V. Filippov, A. Sayir, J. Mater. Sci. 39 (19) (2004) 5987–5994.
[9] Y.B. Paderno, V.B. Filipov, V.N. Paderno, A. Sayir, J. Eur. Ceram. Soc. 25 (8) (2005) 1301–1305.
[10] C.-M. Chen, W.-C. Zhou, L.-T. Zhang, J. Am. Ceram. Soc. 81 (1) (1998) 237–240.
[11] C.-M. Chen, L.-T. Zhang, W.-C. Zhou, J. Cryst. Growth 191 (4) (1998) 873–878.
[12] P.I. Loboda, Powder Metall. Met. Ceram. 39 (9–10) (2000) 480–486.
[13] I. Bogomol, T. Nishimura, O. Vasylkiv, Y. Sakka, P. Loboda, J. Alloys Compd. 485 (1–2) (2009) 677–681.
[14] P. Loboda, G. Kisla, I. Bogomol, M. Sysoev, O. Karasevskaya, Inorg. Mater. 45 (3) (2009) 246–249.
[15] I. Bogomol, O. Vasylkiv, Y. Sakka, P. Loboda, J. Alloys Compd. 490 (1–2) (2010) 557–561.
[16] P. Loboda, I. Bogomol, M. Sysoev, G. Kysla, J. Superhard Mater. (translation of Rus: Sverkhtverdye Materialy) 28 (5) (2006) 28–32.
[17] P.I. Loboda, V.Ya. Shlyuko, V.V. Kovylyaev, Powder Metall. Met. Ceram. 40 (3–4) (2001) 187–199.
[18] W. Martienssen, H. Warlimont (Eds.), Springer Handbook of Condensed Matter and Materials Data, Springer Berlin Heidelberg, Berlin, 2005.
[19] V. Matkovich, Boron and Refractory Borides, Springer-Verlag, Berlin, 1977.
[20] A. Kelly, G.W. Groves, Crystallography and Crystal Defects, Longman, London, 1970.
[21] D. Hull, D.J. Bacon, Introduction to Dislocations, 4th ed., Butterworth, London, 2001.
[22] R. Elliot, Eutectic Solidification Processing: Crystalline and Glassy Alloys, Butterworths, London, 1983.
[23] R.L. Ashbrook, J. Am. Ceram. Soc. 60 (9–10) (1977) 428–435.
[24] H. Deng, E.C. Dickey, Y. Paderno, V. Paderno, V. Filippov, J. Am. Ceram. Soc. 90 (8) (2007) 2603–2609.
[25] R.W.K. Honeycombe, The Plastic Deformation of Metals, St. Martin's Press, New York, 1968.
[26] T.H. Courtney, Mechanical Behaviour of Materials, McGraw-Hill, Columbus, 2000.